buildings

MDPI

Article

Evaluation of the Ultimate Collapse Load of a High-Voltage Transmission Tower under Excessive Wind Loads

Giacomo Vettoretto, Zongchen Li * and Christian Affolter

Mechanical Systems Engineering, EMPA Swiss Federal Laboratories for Materials Science and Technology, 8600 Duebendorf, Switzerland

* Correspondence: zongchen.li@empa.ch

Abstract: Several high-voltage transmission towers failed under excessive wind loads in a mountainous and exposed area. This study discusses the efficient and reliable modeling of lattice towers dominantly loaded by wind, a scenario which led to a collapse cascade in a high-voltage transmission line. The ultimate load-bearing capacity had to be estimated and the failure positions identified. Finite Element Analysis was employed through static analyses, Linear Buckling Analyses (LBA) and RIKS analyses (Arc-Length method) in Abaqus 2021. With the purpose of improving the accuracy in the simulation of structural instabilities of complex lattice structures, the model sensitivity to superimposed geometrical imperfections and the joint stiffness of the truss connections were investigated in brace and lattice structure sub-assemblies. Afterwards, linear analyses and non-linear analyses with imperfections were performed on the single tower model. The analysis proved that solely excessive wind can cause such failure on the lattice structures, and the critical structural elements have been correctly identified. The investigation proved that the towers had not been under-designed with respect to the standards valid at the time of erection. However, they were not designed for this exceptional storm event, and evidence was provided that wind alone could bring about the collapse. It is nevertheless not recommended to increase the safety factors in general for the design of such structures, but to base the assumed loading on actual and local wind and service load measurements.

Keywords: lattice structures; Finite Element Analysis (FEA); structural instabilities; linear-buckling analysis LBA; post-buckling analysis

check for updates

Citation: Vettoretto, G.; Li, Z.; Affolter, C. Evaluation of the Ultimate Collapse Load of a High-Voltage Transmission Tower under Excessive Wind Loads. *Buildings* **2023**, *13*, 513. https://doi.org/10.3390/buildings13020513

Academic Editor: André Rafael Dias Martins

Received: 5 January 2023
Revised: 24 January 2023
Accepted: 1 February 2023
Published: 13 February 2023

Copyright: © 2023 by the authors. Licensee MDPI, Basel, Switzerland. This article is an open access article distributed under the terms and conditions of the Creative Commons Attribution (CC BY) license (https://creativecommons.org/licenses/by/4.0/).

1. Introduction

On 29 October 2018, four lattice towers of the high-voltage power transmission line over Albula Pass, Switzerland, collapsed in a cascade sequence due to an extreme windstorm event. The four lattice steel pylons were found lying in a perpendicular direction with respect to the line, as shown in Figure 1. Tower No. 22 had failed at mid-height, while the others had failed at their basements, suffering severe localized damage, which is generally a sign of a catastrophic and sudden event with high energy. No ice nor snow was found on the structures after the event, and the ceramic insulators and wires were mostly intact. This led to the hypothesis that the wind alone could have been the main cause, which had never previously been observed in Swiss power transmission lines. The investigation had to provide evidence that the towers had not been under-designed at the time of construction, and that a sole exceptional wind event could lead to the observed failure. The actual load capacity at the time of the event had to be determined by simulation, assuming that corrosion or ageing (embrittlement) of the material had played a negligible role.

Overhead transmission lines are a vital component in the correct functioning of the electric power grid. When a failure of even a single tower takes place, the damage can be extensive, involving adjacent towers along the line, and costly, in terms of repair, power disruption and litigation. (Campbell et al. [1], Hoffmann et al. [2]).

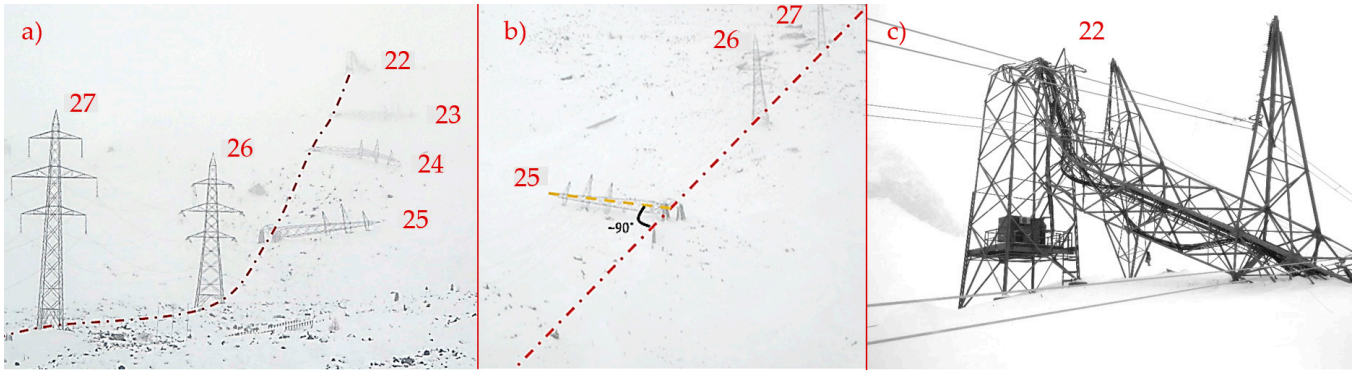


Figure 1. Pictures after the storm in 2018: (**a**) towers from No. 22 to No. 26. Marked in red, the line path: towers No. 22 to No. 25 fallen perpendicularly to the line direction, No. 26 (tensioning tower) and No. 27 still intact; (**b**) arial view of tower No. 25: highlighted, the angle with respect to the tower axis; (**c**) close-up view of tower No. 22: note how the tower has failed at mid-height, and the base is still intact.

Lattice transmission towers are built with eccentrically connected members, which are usually joined with bolts or welds (Fang et al. [3]). During the design phase, stress calculations are obtained via simple linear elastic analysis, in which members are assumed as pinned in place and axially loaded in the name of more conservativeness. The member limit strength according to design standards (EN 1993-1-1 [4], EN 1993-3-1 [5], EN 50341 [6], RS 734.31 [7], SIA 261/1 [8]) is usually given as structural instability load, which is a function of the slenderness as well as the joint type and stiffness (single- or double-bolted connections). A second-order analysis, accounting for the structure deformation under load in the computing of the forces and displacement (geometrical non-linearities), is mandated for structures of this kind and is usually performed with design software (such as PLS-CADD [9]), but it still considers the joints as pinned.

However, the validation of the models through full-scale testing (expensive and thus only regarded as a design check) often shows member behavior far from the pinned hypothesis by manifesting the effects of bending stresses passing through the joints. This can lead to incorrect prediction of the failure mode and the structural capacity. Moreover, the instability limit might not coincide with the ultimate load capacity of the structure, and experimental studies on bolted members (Kettler et al. [10], Kettler et al. [11]) show discrepancies with respect to the design rules, offering alternative solutions that better include joint stiffness and imperfection modes into the equation.

A less conservative (or more realistic) approach is preferred for a failure analysis: by proving that the structure with its true mechanical strength (i.e., above the guaranteed values from standards) can fail under realistic loading, it is possible to confirm that it has to fail with minimal guaranteed material properties under the same conditions. Furthermore, in large lattice structures, the ultimate load-bearing capacity might not coincide with the instability load of the weakest member (design load capacity limit), whereas the actual tower could comprise a plastic reserve in the post-instability phase, or redundant structural elements could lead to a load redistribution (i.e., a changing load path).

A way to perform such an analysis correctly and cost-effectively is to use Finite Element Methods (FEM), accounting for geometric non-linearities, cross-section yielding (material non-linearities), stiffness in the joints and imperfection modes. Many authors have addressed the modeling of lattice structures. Albermani et al. [12] advocate the use of non-linear analysis as a tool to improve design accuracy and failure mode prediction, aiming to reduce the need for full-scale testing. Their in-house code, which accounts for geometrical and material non-linearities, has been used to conduct analysis on different load cases on a high-voltage transmission tower and has predicted the same buckling mode and load (relative error within 1.2%) as the test result, although not including geometrical imperfections nor joint compliance (finite stiffness). Alminhana et al. [13] adopted the

non-linear method from [12] in their transmission line cable rupture time-response analysis, obtaining results within ±12% of the test data.

Wang et al. [14] introduced the Eigenmode Assembly Method (EAM) based on the superposition of multiple imperfection modes obtained from a Linear Buckling Analysis (LBA), obtaining buckling loads between 82 and 125% of the nominal value (design standard load case) depending on the single buckling mode with different imperfection magnitudes, and between 102% and 118% with EAM. Affolter et al. [15] analyzed the collapse of a high storage rack due to structural instability by means of Finite Element Analysis (FEA) using Abaqus v6.7. Imperfection modes obtained from an LBA, as well as local geometrical imperfections (dents) and load imperfections, were applied when determining the collapse load of the structure, showing a large sensitivity on the collapse load (up to 32% less than the "ideal nonlinear" case).

Rao et al. [16] achieved 3–14% error with respect to a transmission tower test using the Arc-Length method in a non-linear FE analysis, accounting for both geometrical and material non-linearities. However, the failure location is not well matched, probably due to the joints considered as pinned. In further studies of theirs [17,18], they described the force–displacement curve and rupture position within the same range of accuracy.

Darestani et al. [19] analyzed the impact of non-linear material and geometry, imperfections, joint flexibility and failure, as well as stochastic uncertainties, in a push-over analysis using commercial FE software, with the purpose of determining the influence of model details on the load-bearing capacity under the specific load case. Just by including joint flexibility, the ultimate load capacity decreased, on average by 3% in the transverse wind case, and 6% in the longitudinal wind case. The tip displacement at ultimate load increased by 13% and 12%, respectively.

Most of the presented techniques, alongside novel proposed approaches, were combined and used in the current study with the purpose of improving the accuracy in the prediction of the load-bearing capacity and failure mode of the Albula Pass towers in a conservative manner (from the perspective of failure analysis). The limits of numerical recalculation of a complex lattice structure should be explored, using methods that are not necessarily available (or applied) in the design process.

2. Materials and Methods

Based on the aforementioned mentioned work, model imperfections [14,15,19], non-linearities (both geometrical and material) [12–19], and joint stiffness (as opposed to a "fixed" or "pinned" approach, [19]) were introduced in the analysis. Moreover, the models were built with different element types and combinations that better suited the tasks. Abaqus 2021 [20], as a general-purpose three-dimensional (3D) FE tool, offers different possibilities of non-linear analysis procedures to address the present problem, including:

- "Linear Perturbation, Linear Buckling Analysis" (LBA): This is based on the structural linearity theory (small displacements, linear elastic material, definite stiffness matrix); the solution is the series of eigenvalues of the introduced perturbations that make the system unstable (when stiffness matrix equals zero). However, it does not mean that the ultimate load of the structure is always the one that causes instability.
- "Dynamic, Implicit": This procedure includes the dynamic equation into the implicit solver. The large time increments reduce the computational cost for long dynamic simulations, but they could miss high-frequency dynamics. In Abaqus 2021, a maximum increment length can be set in order to improve accuracy, which, however, increases the computational cost massively.
- "Dynamic, Explicit": This finds the exact solution of the next increment state which is a direct function of the previous one (at a very low computational cost) and naturally requires a very small time increment (proportional to mesh size and inversely proportional to sound propagation) in order to solve the equation. It shall instead be used for high-frequency dynamics, but can be computationally expensive for long simulations and fine mesh.

- "General, RIKS": The increment is arc length-based (the so-called Arc-Length method), which uses the length of the path between two increments in the force–displacement curve, decoupling the proportionality and direction of the force and displacement increase (Figure 2). Thus, this approach is able to overcome the instability point and show the post-bifurcation behavior.

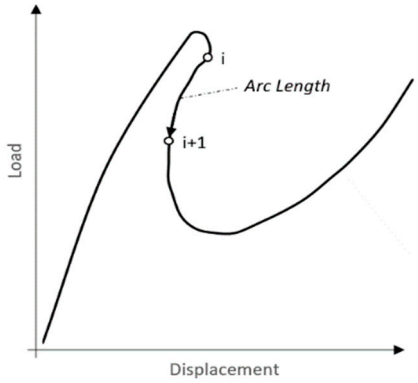


Figure 2. Arc-Length increment displayed in a typical force–displacement curve.

When analyzing a structure with a monotonic force–displacement curve, the ultimate load capacity and the full force–displacement curve can be obtained with displacement-controlled "General, Static", "General, RIKS" or "Dynamic, Implicit" procedures. In the present case, the LBA is adopted in the model of the failure analysis as a first hint on the instability load, and the scaled buckling mode shapes are then used to introduce model imperfections in a complete RIKS analysis, estimating the actual load-bearing capacity and simulating the post-instability behavior. A push-over analysis by means of the "Dynamic, Explicit" procedure is a possible alternative for the RIKS analysis.

3. Modeling Strategies

3.1. Material Model, Mesh Size and Element Type Effects

Geometric non-linearities (large displacements) are already included by default in most analysis procedures of Abaqus 2021 [20]. Material non-linearities, element types and mesh size can potentially affect the results of an FE analysis. To address those concerns, a sensitivity study was conducted on a simple L-section column model with pinned/fixed ends (see Figure 3).

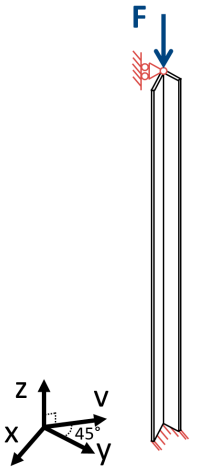


Figure 3. Diagram of a pinned–fixed column under compression.

A previous study provided the material engineering curve from tensile testing on specimens collected from the towers after the accident in Albula Pass. Based on the resulting properties, the following models were analyzed (stress–strain curves in Figure 4):

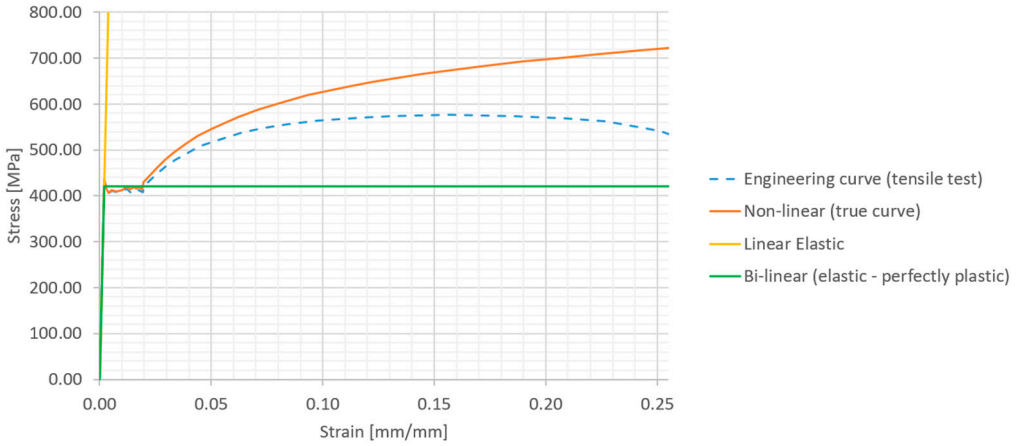


Figure 4. Material characteristic for the different models, alongside the engineering curve from the tensile test.

- linear elastic (with Young's modulus of 210 GPa, Poisson's ratio of 0.3);
- bi-linear (with a yield strength of 420 MPa, simplified as elastic/perfectly plastic);
- non-linear (true stress–strain curve, converted from engineering values).

As Uriz et al. [21] suggest, at least 3–4 elements per flange (for both shell and solid) and 3 elements in thickness (for solid) are necessary to reliably simulate buckling. Solid, shell, and beam element types were compared (Table 1) with different mesh sizes (from 13 to 380 elements per beam length, 1 to 10 elements per flange for shell and solid and 1 to 3 elements in thickness for solid). The results are shown in Figure 5.

Table 1. Buckling modes reproduced by each element type in an LBA (examples of the buckling modes can be found in Figure 6).

Element Type	Flexural, v Axis		Flexural, x or y Axis		Torsional	Flexural–Torsional	
	Mode 1	Mode 2	Mode 1	Mode 2	Mode 1	Mode 1	Mode 2
Beam	yes	yes	yes	yes	no	no	no
Shell	yes	yes	no	no	yes	no	yes
Solid	yes	yes	yes	no	yes	yes	yes

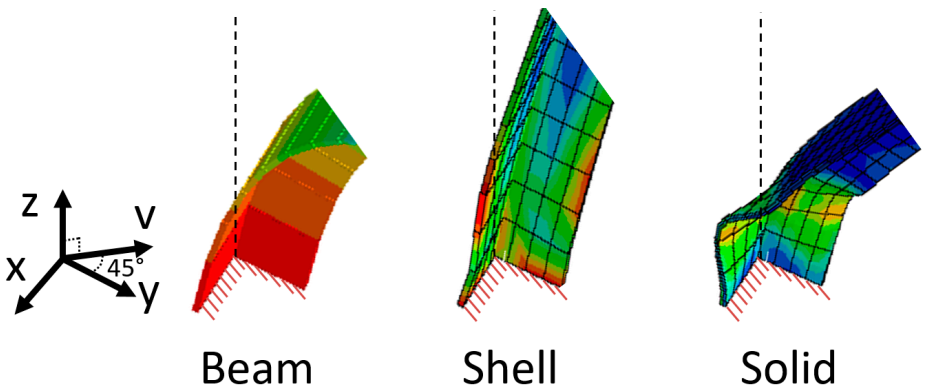


Figure 5. Local deformation shown at the beam's fixed end. (Color from blue to red represents the value of equivalent stresses from low to high).

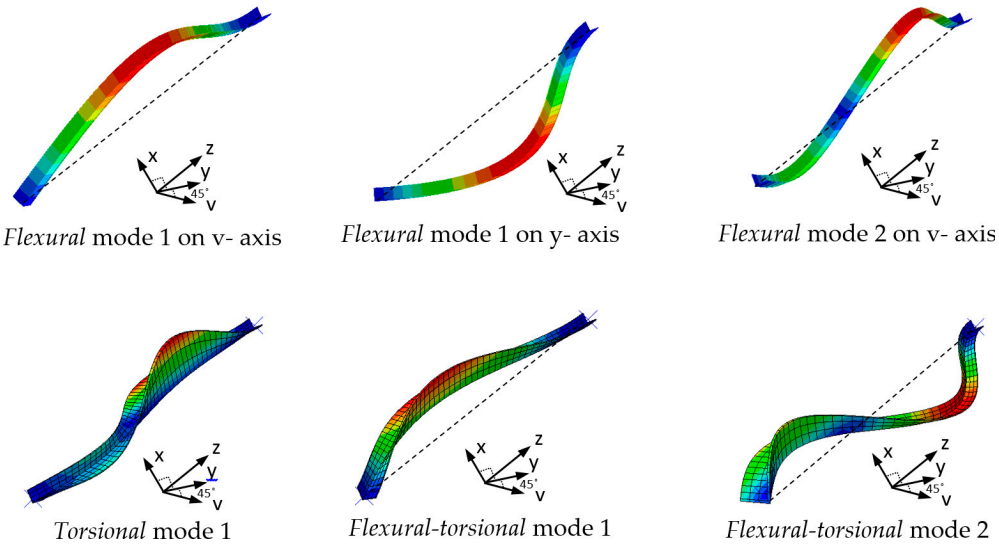


Figure 6. Examples of buckling modes reproduced in an LBA. Flexural modes are characterized by bending in axis x, y or v. Axis x and y are aligned with the flanges; v axis (the one with the weakest moment of inertia) lies 45° to y axis in the x-y plane. The torsional modes have angular deformation in the z-axis, whereas torsional–flexural modes combine it with bending. (Color from blue to red represents the value of equivalent stresses from low to high).

A bi-linear model was sufficient to show the material non-linearity effects and section yielding in the elastic and inelastic buckling areas. The sensitivity to the mesh size and type confirmed the findings of P. Uriz et al. [21]. The local buckling of the flanges can be properly displayed only with fine meshed solid or shell elements. Furthermore, the beam elements do not show any buckling mode other than flexural, while the other element types display torsional and torsional–flexural buckling. The number of elements in the length affects mostly the ability to display local deformation. These mesh types are going to be used in the following—Sections 3 and 4—when referring to a specific type of element:

- 3D solid—quadratic reduced integration: 5 elements per flange width, 3 elements per thickness and 100 elements per member length (biased towards the edges). In detailed regions, such as the bolt position, the number of elements per width is going to be increased up to 20.
- 3D shell—linear reduced integration: 6 elements per flange width; mid extrusion: 60 elements per member length (biased towards the edges).
- 3D beam—linear: 40 elements per member length.

3.2. Sensitivity to Imperfections

As analytical buckling formulas such as Euler and secant formulas (as shown by Ferdinand P. Beer in [22]) are based on small displacements and linear elastic theory, and design standards might contain intrinsic conservativeness; validation of the FE model should be based on experimental results. However, in most experimental setups, the condition of the beam's end-restraints and the initial imperfections are often overlooked (i.e., bolt type and design, imperfections direction and magnitude), which can lead to the incorrect modeling of the structure.

Experimental results from Kettler et al. [10] were used to validate the present FE models, as they include more information regarding the imperfection modes and the bolt connections design. The validation of experiment C1 from [10] is reported as an example.

An L80x8 column, 3.17 m in length, was pinned between two clamped gusset plates via single-bolt connection. The measured beam imperfection was $e_{imp} = L/2918$, but no imperfection direction is given. The beam was modeled with bi-linear elastic material with an elastic modulus of 210 GPa and a yield limit of 333.9 MPa; the gusset plate and bolts were linear elastic, as in Ref. [10]. The 3D solid elements were used for the entire assembly,

following the guidelines in Section 3.1. The bolt connection was designed according to Eurocode 1993-1-8 [23].

Darestani et al. [19] and P. Uriz et al. [21] used a sinusoidal imperfection (maximum displacement at the center of the element) of 0.05–0.1% of the length (e_{imp} = *L/2000* to e_{imp} = *L/1000*). Wang et al. [14] employed the Eigenmode Assembly Method (EAM) based on the superimposition of multiple imperfection modes obtained from an LBA. Note that according to *buckling curve b*, EN 1993-1-1 [4], a standards imperfection magnitude, is e_{imp} = *L/250* for elastic analysis, and e_{imp} = *L/200* for plastic analysis.

Models with different imperfection magnitudes (and directions), bolt tensions and friction coefficients were considered (Table 2, Figure 7) in order to match the experimental data and understand their influence on the structural instability mode and load.

Table 2. Analyzed models of L80x8 beam section. The model codename refers to bolt tension (ratio to Eurocode 1993-1.8 design value), applied imperfection mode, imperfection magnitude, and friction coefficient.

Model Name	Bolt Tension [% w.r.t. Design [21]]	Imperfection Type	Imperfection Magnitude [L/e_{imp}]	Friction Coefficient [−]
100-1-300-0.25 (as in [10])	100%	1st mode	300	0.25
100-1-1350-0.25	100%	1st mode	1350	0.25
100-EAM-300-0.25	100%	EAM (1, 2, 3)	300	0.25
75-1-300-0.25	75%	1st mode	300	0.25
115-1-300-0.25	115%	1st mode	300	0.25
125-1-300-0.25	125%	1st mode	300	0.25
100-1-300-0.35	100%	1st mode	300	0.35
100-EAM-300-0.35	100%	EAM (1, 2, 3)	300	0.35
115-1-300-0.35	115%	1st mode	300	0.35
115-EAM-300-0.25	115%	EAM (1, 2, 3)	300	0.35
115-EAM-300-0.35	115%	EAM (1, 2, 3)	300	0.35

The numerical results show lower initial axial stiffness compared to the experimental curve in Figure 7, but the deflection in the failure direction is well matched, undergoing the same failure mode. The single-bolt connection always slips with friction coefficient f = 0.25; the models with increased friction coefficient or bolt force better reproduce the experimental curve.

The results showed a large scatter in the ultimate load capacity estimation (between +17.2% and −13.3%, with respect to the experimental value [10]); they largely depend on the type and magnitude of imperfections. A lower initial imperfection gives a lower capacity, due to the superimposed buckling mode being in the opposite direction to the actual failure.

The most accurate models are the ones with EAM imperfections and a slightly increased bolt force or friction coefficient (such as 115-EAM-300-0.25 and 100-EAM-300-0.35, Table 3). For this reason, EAM imperfections were next applied to the lattice subassemblies in Section 3.4.

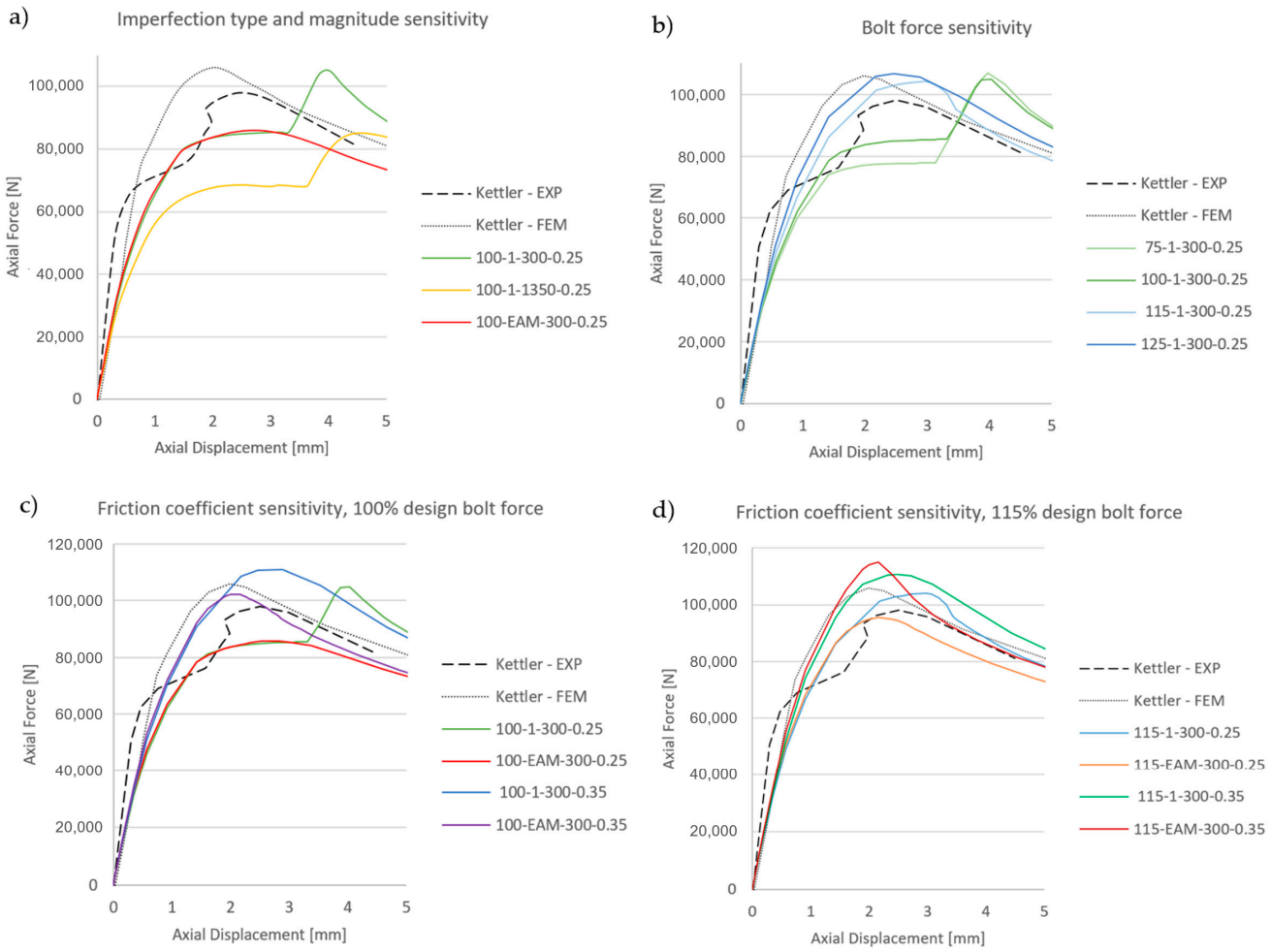


Figure 7. Axial force–displacement curves of the FE models described in Table 2, compared to the experiment [10]: (**a**) imperfection type sensitivity; (**b**) bolt force sensitivity; (**c**) friction coefficient sensitivity with bolt force 100%; (**d**) friction coefficient sensitivity with bolt force 115%.

Table 3. Ultimate load capacity comparison to the experimental results [10].

Model	Kettler [10] Experiment	100-1-300-0.25 (as in [10])	100-1-1350-0.25	100-EAM-300-0.25	75-1-300-0.25	115-1-300-0.25	125-1-300-0.25	100-1-300-0.35	100-EAM-300-0.35	115-1-300-0.35	115-EAM-300-0.25	115-EAM-300-0.35
Ultimate capacity (kN)	98.1	105.0	85.0	85.9	107.0	104.2	106.8	111.0	102.3	110.7	95.5	114.9
Difference w.r.t. experiment (%)	/	7.0%	−13.3%	−12.5%	9.0%	6.2%	8.8%	13.2%	4.2%	12.8%	−2.7%	17.2%

These findings are supported by the studies of Wang et al. [14], who found that, depending on the type and magnitude of the applied initial imperfection, the buckling capacity of tower members can vary by up to 16% for the same failure mode. Similarly, C. Affolter et al. [15] found a difference of around 10% in structure ultimate load estimation, depending on the applied mode.

3.3. Boundary Condition Simplification

Structural instabilities are by definition sensitive to boundary conditions. In a lattice structure, the members are connected to each other, thus the load sharing and the flexibility of the joints is of extreme importance.

Kettler et al. [11] introduced a systematic procedure to model and validate the end-constraints, i.e., the joint compliance, effectively replacing the 3D-joints with equivalently stiff or compliant ends. A similar approach was employed, involving:

(1) the validation of a detailed FE model (in which geometric imperfections, bolt force, slippage and friction are simulated) using experimental tests;
(2) the development of equivalent joint stiffness functions, as shown in Figure 8, by applying the reference load in every degree of freedom of the FE end model;
(3) the application of the stiffness functions at the beam-ends and validation of the model by comparison with experimental tests and complete geometry FE results.

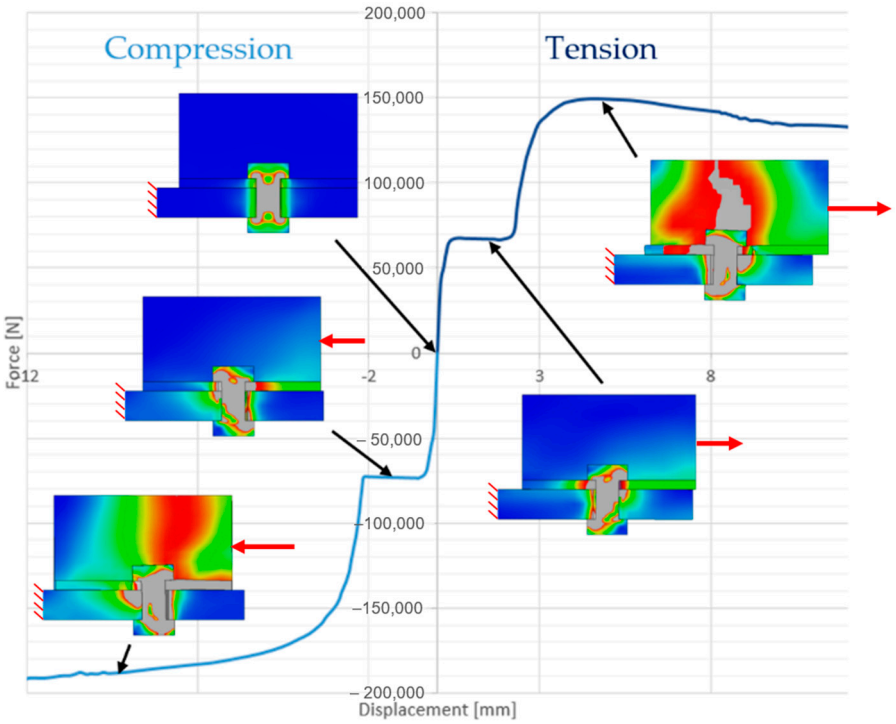


Figure 8. Example of load–displacement curves (stiffness functions are their derivative with respect to displacement) for tension and compression in a single bolt joint (in grey: the elements over the limit at 420 MPa). (The direction of the arrows represents the direction of loads, and the color from blue to red represents the equivalent stress value from low to high).

In order to simulate what happens at the member-ends, the "wire connector" elements were used: in Abaqus 2021, they simulate a kinematic relationship between two nodes. They are usually employed for substituting bolts and rivets with stiffness functions in order to simplify the FE model. The following stiffness models were applied to this type of element in the FE models:

- linear: initial linear stiffness coefficient;
- non-linear: complete force–displacement curve/stiffness function for every degree of freedom (developed as in Figure 8);
- rigid: fixed;
- pinned;
- rigid + pinned: with the only free rotational degree of freedom around the bolt axis (no stiffness applied).

It should be noted that there are four main limitations to this approach: the local deformations close to the joint are misrepresented; multiaxial loading which cannot be properly simulated by mere uniaxial stiffness functions; the lack of a time-dependent effect, such as dynamic friction or damping; and that imperfections cannot be superimposed.

The basic brace model was modeled with shell elements. The brace model with non-linear joints was also meshed with solid and beam elements. The reference was chosen as model 100-1-300-0.25 from Section 3.2, with 3D-joints and contact properties (calibrated in Section 3.2), which have the same input parameters as Kettler [11], are closest to the experimental results (Table 3) and showed the slip at the bolted connections (thus, it is more compelling from a "demonstrator" standpoint). The 1st mode buckling imperfections of the magnitude $e_{imp} = L/300$ were used in each model.

The force–displacement curves (see in Figure 9) show that the slippage of the joints in the non-linear stiffness models is similar to the 3D-joints reference. The difference in displacement at the ultimate load between the models with slip (non-linear stiffness and the reference), compared to the one without, is in the order of 2 mm, close to the bolt clearance in the joint. In all the analyzed cases, the failure mode is similar to the reference and the real counterpart (buckling in the y axis, Figure 10), except for the pinned joint models, which suffer from buckling in the axis of the weakest moment of inertia (v axis, as in Figure 5), and thus has a much lower ultimate load capacity. Notice how, even though they do not display the entirety of the behavior, the rigid + pinned or linear models are in line with the others in terms of ultimate capacity (Table 4). Moreover, there is little difference whether the brace is modeled with solid, shell or beam elements when using the non-linear joint model: under the same boundary conditions, and if the buckling mode is not local, the element type does not considerably affect the brace's failure mode and ultimate load capacity.

Note that, as already shown in Section 3.2, large variability in the ultimate load capacity also comes from the mode and magnitude of the applied imperfections, so there might be a slight difference depending on whether the imperfection is applied to the entire model or to the brace only (imperfections cannot be applied to connector elements in Abaqus 2021).

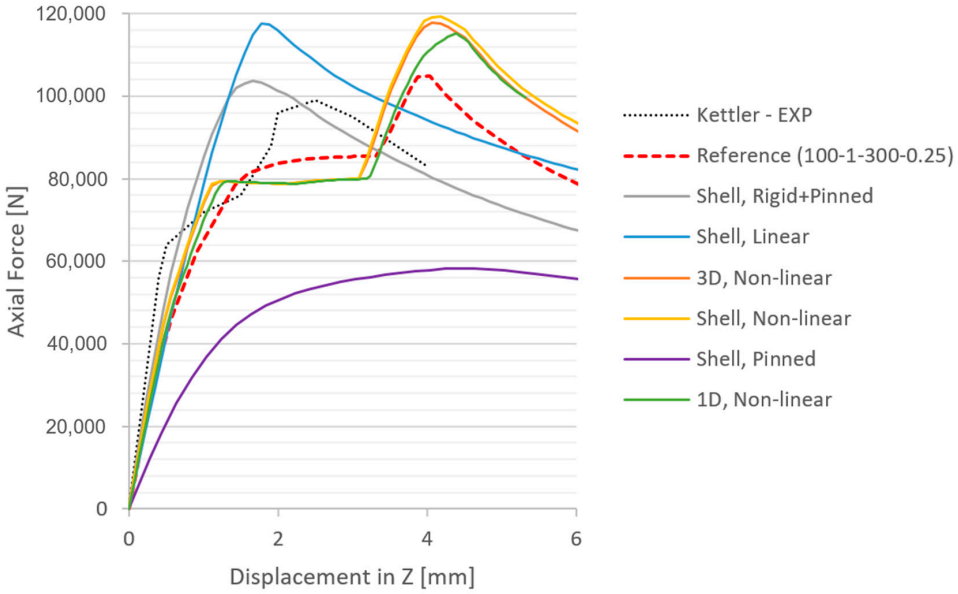


Figure 9. Axial force–displacement curves of the stiffness models compared to the experiment [10] and the reference (100-1-300-0.25).

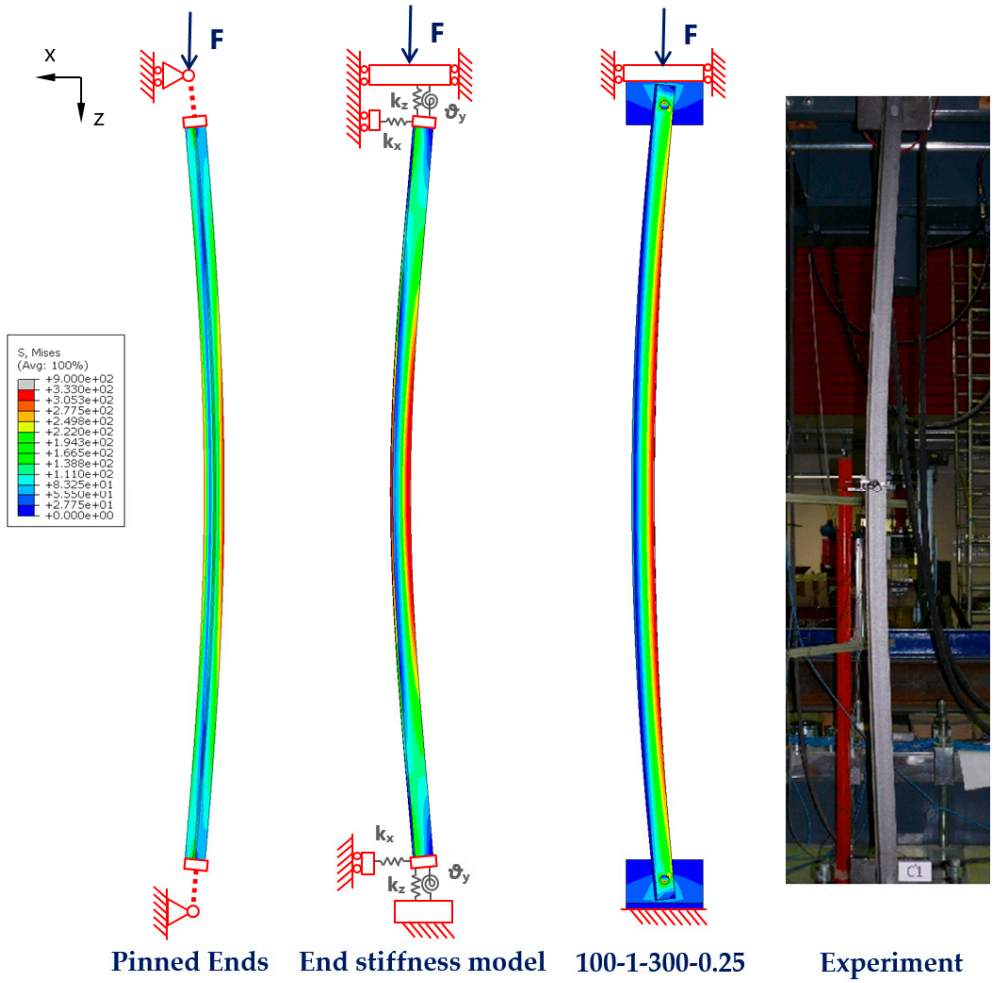


Figure 10. Comparison of the deformed models upon ultimate capacity load. From left to right: the pinned model, the compliant joint model (with the fictitious linear and rotational springs to symbolize the wire connector elements), the FE reference (100-1-300-0.25) and the real counterpart from [10]. Notice how no part of the brace section is yielding, a sign that the failure mode is elastic buckling.

Table 4. Load capacity of the models compared.

	Reference (100-1-300-0.25)	Shell, Pinned	Shell, Rigid + Pinned	Shell, Linear	Solid, Non-Linear	Shell, Non-Linear	Beam, Non-Linear
Load capacity [kN]	105.0	58.3	103.7	117.6	117.8	119.2	115.1
Rel. error [%]	/	−44.5%	−3.0%	+10.0%	+10.2%	+11.5%	+7.7%
Displacement at ultimate load [mm]	4.05	4.43	1.76	1.82	4.11	4.17	4.42

3.4. Modeling of Lattice Structures

The modeling strategies developed on the brace model from Section 3 were applied to a planar sub-assembly and to a 3D-subassembly in order to test their effectiveness on more complex structures, and ultimately to choose the optimal way to model the entire lattice tower. Please note that experimental references for the two cases were not considered due to project time and budget limitations.

3.4.1. Planar Subassembly

Similar to a tower section face, single-bolt connections have been placed in the horizontal braces and double for the diagonals when attached to the main legs. Dimensions and geometry are given in Figure 11. The reference was built entirely with 3D solid elements,

and is able to simulate the contact interaction in the joints (similarly built as model 100-1-300-0.25 from Section 3.2). The models with both shell and beam elements, with connectors (linear, non-linear, pinned and rigid + pinned joint models created with the same method as Section 3.3) that replace the joints, all have horizontal braces and the diagonals built with beam elements, whereas the main legs are shell elements. A model made of only beam elements with all members rigidly connected was also built. EAM buckling imperfections of the magnitude $e_{imp} = L/300$ were used in each model.

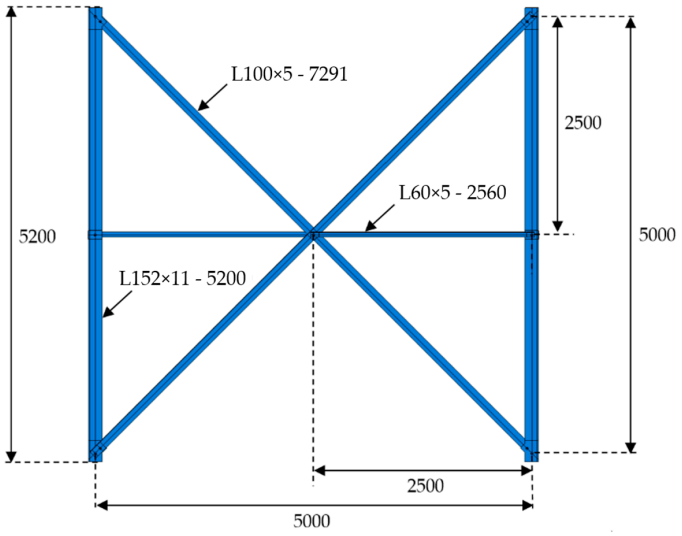


Figure 11. Planar sub-assembly geometry and dimensions.

None of the models showed evidence of joint slippage. The resulting force–displacement curves shown in Figure 12 are almost identical for linear, non-linear, pinned and rigid + pinned connector models, and their ultimate load capacity differs only by 0.6% (Table 5): the buckling is localized in the main legs, thus limiting the load sharing to the diagonals through the joints. In fact, the models with rigid joints appear to similarly match the 3D results. The non-linear model shows a slight increase in displacement at the ultimate load (+1.5%). In general, the shell + beam strategy gives results that are between 14% to 18% higher than the others: one reason for this might be the extreme stiffening provided by the stringer elements [20] that connect the diagonals to the legs.

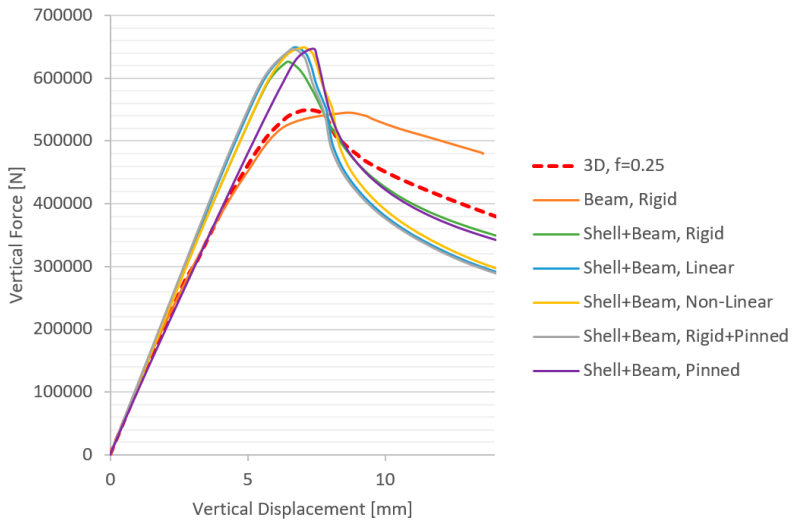


Figure 12. Vertical force–displacement curves of the planar models compared.

Table 5. Load capacity of the planar subassembly models compared.

	3D, f = 0.25 Reference	Beam, Rigid	Shell + Beam, Rigid	Shell + Beam, Pinned	Shell + Beam, Linear	Shell + Beam, Non-Linear	Shell + Beam, Rigid + Pinned
Ultimate load [kN]	549.9	544.4	625.4	647.3	648.1	649.3	646.0
Relative error [%]	-	−1.0%	+13.7%	+17.7%	+17.8%	+18.1%	+17.5%
Displacement at ultimate load [mm]	7.2	8.4	6.4	7.3	6.9	7.0	6.5

3.4.2. 3D Subassembly

A model of a tower segment was made for the 3D-subassembly, with similar geometry and member sections as the planar model (Figure 13). Three different modeling strategies were adopted in a similar configuration to the planar model, using the beam with rigid joints, the shell and beam with rigid joints (arranged as the planar subassembly) or the shell and beam connected by connector elements (with linear, non-linear, pinned and rigid + pinned connections, similarly to the single brace model in Section 3.3). However, due to assembly constraints, it was not possible to build a 3D reference; hence, the applied modeling strategies were based on the previous sections and further simplified. EAM buckling imperfections of the magnitude $e_{imp} = L/300$ were applied on the structure. The results are summarized in Figure 14 and Table 6.

Table 6. Load capacity of the 3D-subassembly models compared.

	Beam, Rigid	Shell + Beam, Rigid	Shell + Beam, Pinned	Shell + Beam, Linear	Shell + Beam, Non-Linear	Shell + Beam, Rigid + Pinned
Ultimate load [kN]	625.4	691.0	520.7	559.1	564.7	662.5
Displacement at ultimate load [mm]	15.5	16.6	15.4	18.5	23.7	19.1

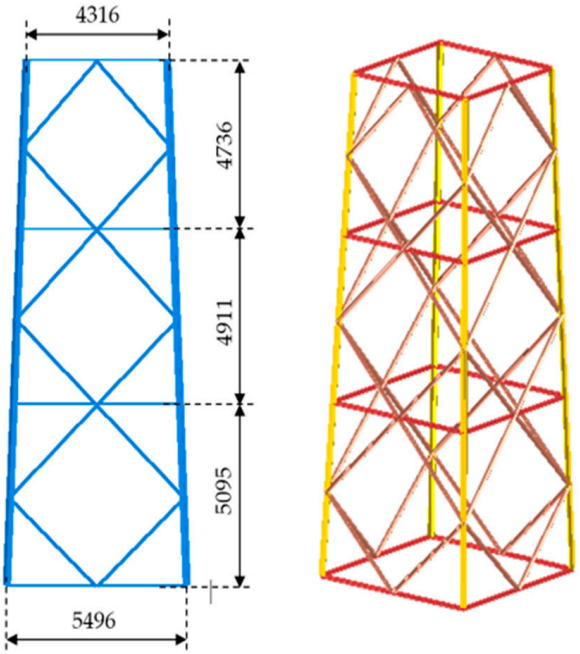


Figure 13. 3D- subassembly dimensions and geometry. On the right-side picture: in pink, the L60x5 section braces; in yellow, the L152x11 main legs; and in red, the 100x5 braces.

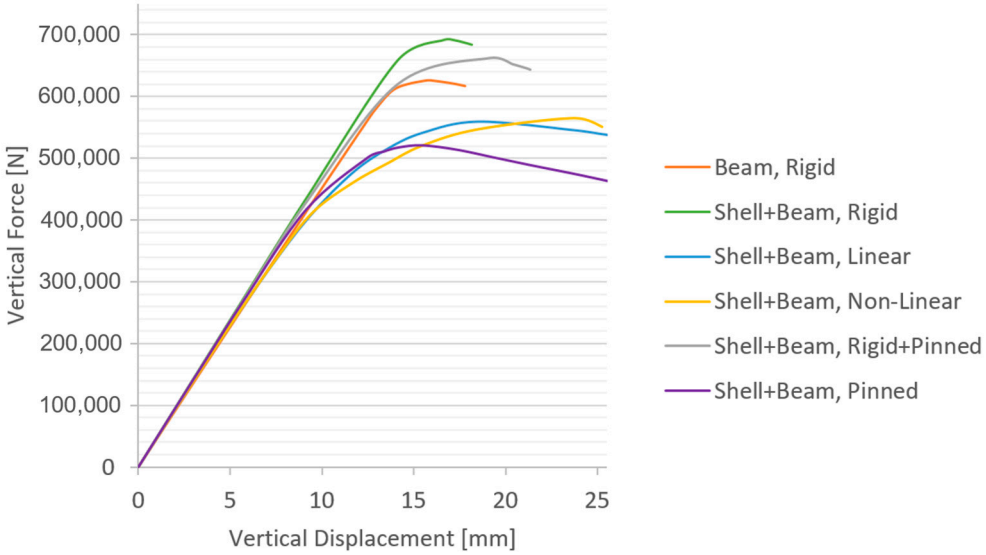


Figure 14. Vertical force–displacement curves of the 3D-subassembly models compared.

In this case, the shell + beam strategy did not show a higher instability load with respect to the beam model. The difference between the models with rigid joints and the ones with connector stiffness was substantial. The models with rigid connectors showed an ultimate load which is higher between 10% and 33% with respect to the pinned, linear or non-linear connector models. There is also a large difference between the linear and the non-linear: the slip increases the displacement at the ultimate load by 28%, without significantly affecting the ultimate load capacity (+1%). This is much more pronounced than what the results from Darestani et al. [19] predicted: a load capacity reduction of 3% and an increase in displacement at the ultimate load of 13% when using flexible joint models accounting for slippage in lattice structures. The cause of the large divergence could be related to the applied EAM imperfections (whereas Darestani [19] applied a single buckling mode imperfection). The model with pinned joints is the one with the lowest load bearing capacity. However, note that it is hard to state which modeling approach is the most accurate, since neither a more detailed 3D model accounting for joint contact and slip nor experimental results were available for analysis and comparison.

For a failure analysis case, shell + beam with rigid joints could be the optimal strategy as it overestimates the strength both in 3D- and planar subassemblies (Section 3.4.1).

4. Tower Ultimate Load Estimation

Various modeling strategies for frame structures were analyzed in Section 3, and the approach that better suits the initially presented failure case was chosen: the tower was modeled with shell + beam with rigid connections in order to be conservative with regard to failure analysis (see Figure 15), and to reduce the modeling effort, as the modeling strategy consistently overestimated the ultimate load capacity in the planar and 3D-subassemblies (Section 3.4).

4.1. Load Case Estimation

There was no kind of measurement system for wind pressure and direction in place during the event; thus, the wind load had to be estimated from the current standards. The possibility of Computational Fluid Dynamics (CFD) simulation was analyzed but discarded due to the lack of data and intrinsic complexity of simulating the airflow in a mountainous area.

Most European and Swiss standards for the design of lattice transmission towers employ a formulation based on base wind pressure (from time-averaged measurements). These values can be found in weather maps such as the ones in SIA 261/1 [8] (see Figure 16).

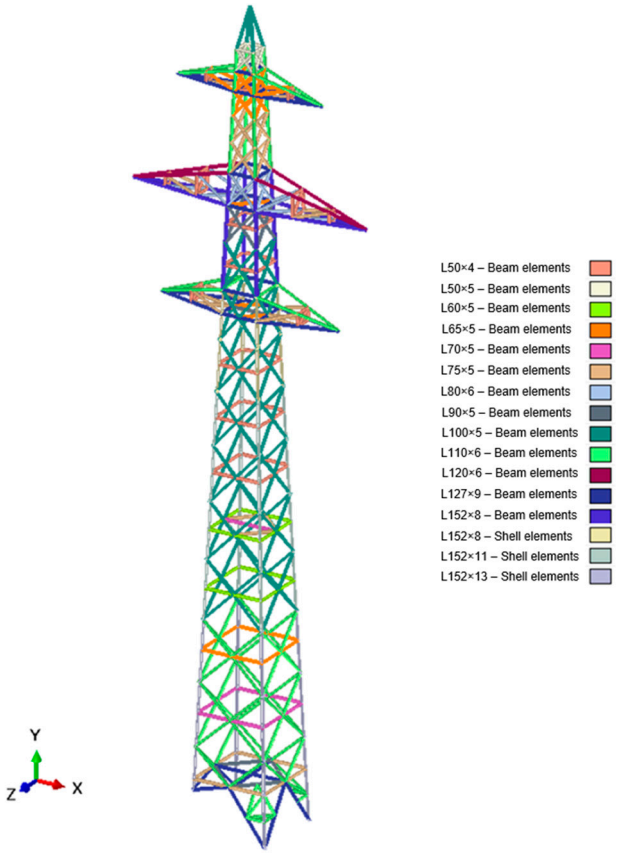


Figure 15. Tower geometry, sections (entirely L-section members, dimensions flange width × flange thickness) and mesh element types (shell and beam).

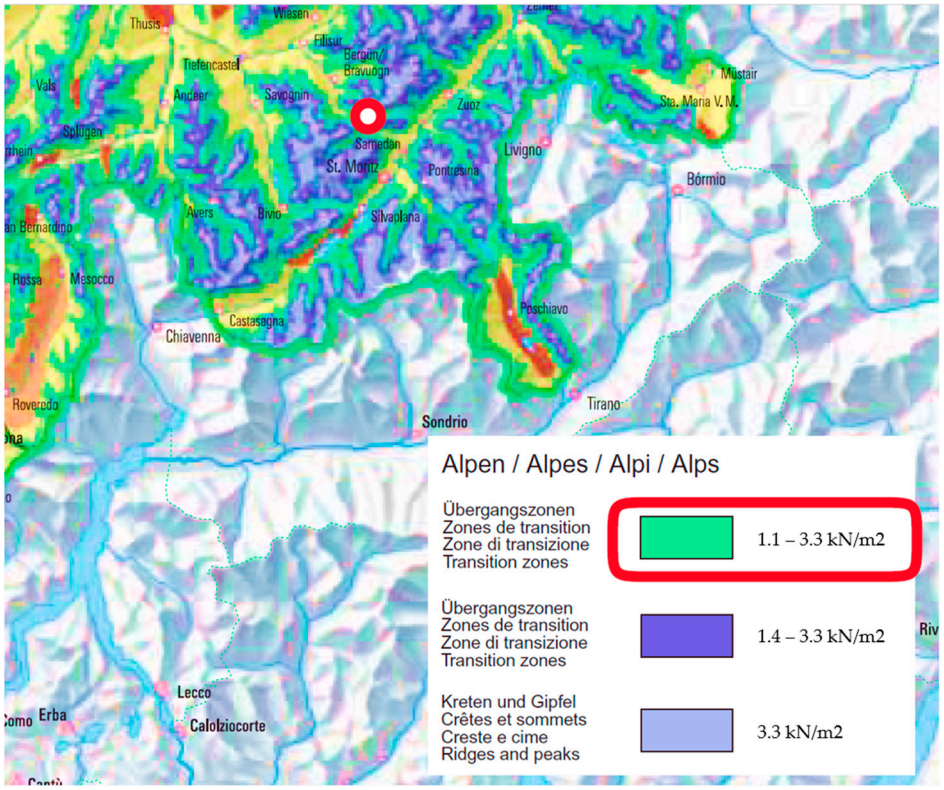


Figure 16. SIA 261/1, appendix E wind pressure map, Albula Pass highlighted [10].

According to the weather maps, the base wind pressure on Albula Pass is 1.1 to 3.3 kPa. For the sake of the failure analysis conservativeness, the lower value of 1.1 kPa was chosen, as it is more realistic (it corresponds to a wind speed of around 45 m/s at an altitude of 2300 m). Note that, in the design process of such structure, a base wind pressure of 3.3 kPa should be the safe choice.

EN 1991-1-4 [24], EN 1993-3-1 [5], EN 50341 [6], RS 734.31 [7] and SIA 261/1 [8] were also employed to calculate the wind loads with a base pressure Q_1 of 1100 kPa. In all these standards, the wind pressure is a function of the height (Figure 17) and can be applied to a level-based subdivision of the structure with the following formulation (based on Figure 18):

$$F_i = Q_{1,i} \cdot (1 + \alpha_i) \cdot A_{p,i} \quad (1)$$

where F is the force applied to the level i, Q_1 the base pressure, α the shielding factor and A_p the projected surface area of the level. Note that, for EN 1991-1-4, the load is much larger if the peak dynamic value is considered. For this study, the mean wind pressure value based on this standard was used instead, which represents the lower value of the realistic range.

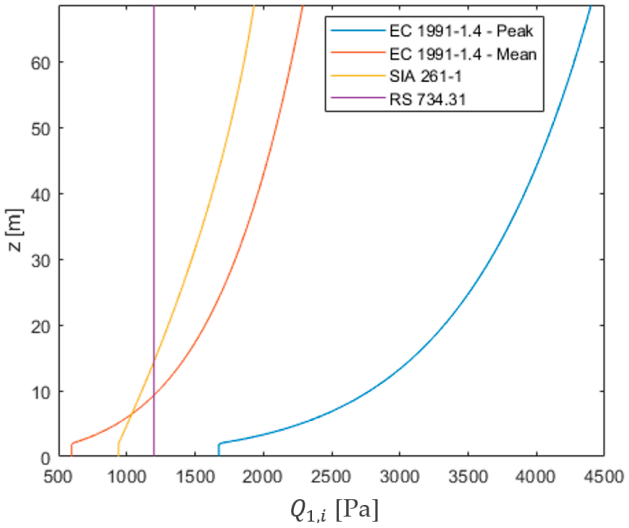


Figure 17. Comparison of different design standards' pressure distributions [7,8,25].

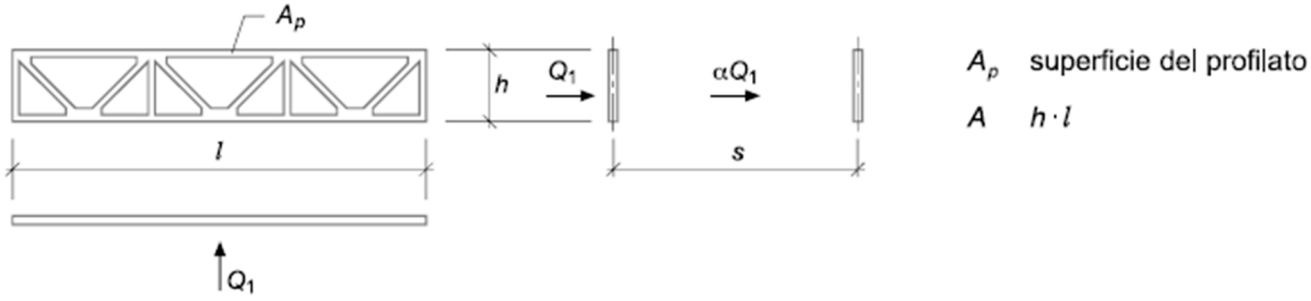


Figure 18. Force application method [8].

Another method wasattempted, using experimentally derived drag and lift coefficients of the individual braces ("Drag and Lift" model in Figure 18): the chosen dataset contained the normalized values of drag and lift coefficients from experiments on an S52x3R beam for the angle sections, as in Prud'homme et al. [25], and test specimen 142-15026-2 for the cables, as in Stroman et al. [26].

$$F_{D,i} = C_D(\alpha_{1,i}) \cdot A_{nom,i} \cdot Q_{1,i} \cdot \cos^2(\alpha_{m,i}) \quad (2)$$

$$F_{L,i} = C_L(\alpha_{1,i}) \cdot A_{nom,i} \cdot Q_{1,i} \cdot \cos^2(\alpha_{m,i}) \quad (3)$$

where F_D is the drag force in wind direction, F_L is the lift force transverse to the wind, α_m is the angle between the wind and the member axis normal plane, α_1 is the angle to the reference wind facing position in the normal plane and A_{nom} the nominal area (section width times length) of the element i.

Similarly, the wind forces on the conductors have been calculated, and were applied to each arm and tip.

The total forces were compared level-wise in Figure 19 and as absolute values in the polar plots of Figure 20, with respect to the wind angle of attack. Note that the variation of the wind angle of attack is not accounted for in the design process required by some standards (RS 734.31 [7]), where the structure only has to be proven to be able to withstand specific load cases (i.e., wind only in transverse direction, combination of wind and ice load, etc.).

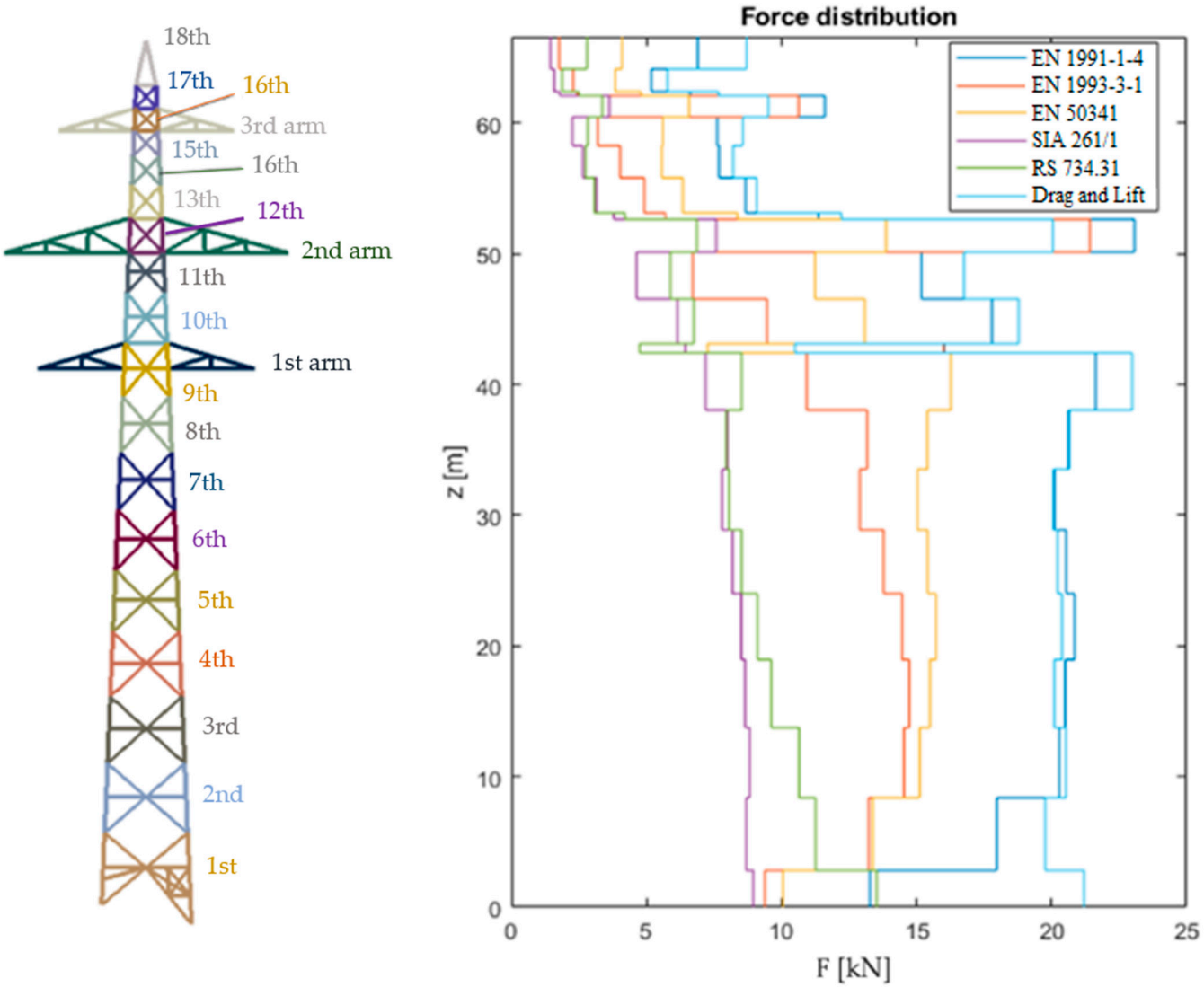


Figure 19. Total forces on each of the sections with purely transverse wind (0°).

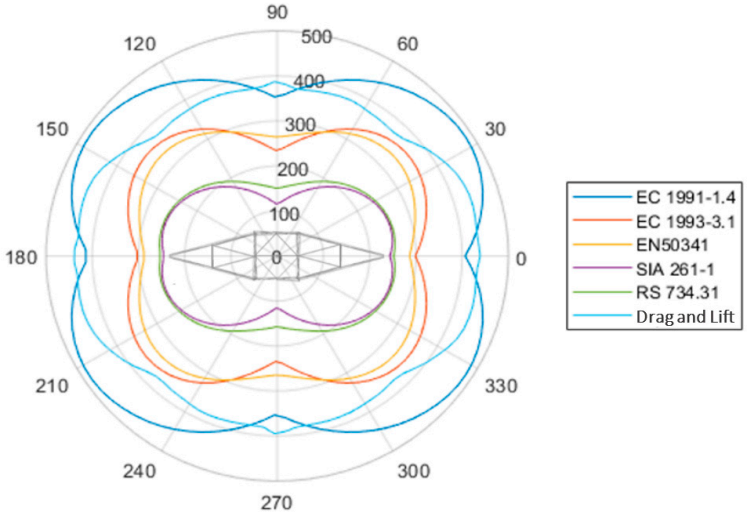


Figure 20. Polar plot of the total lateral forces (in kN, sum of both total wind load on the lattice structure and resultant force from the wind on the cables) according to different standards and depending on angle of attack (deg, 0° in transverse direction).

The maximum total force was located between 20° and 45° in the line transverse direction for most of the standards' wind load models. The European EN 50341 [6], EN 1991-1-4 [24] and EN 1993-3-1 [5] appeared to be much more conservative (design-wise), especially considering that the mean wind pressure was selected instead of the peak dynamic load. The Swiss standards, RS 734.31 and SIA 261/1, produced much lower and more realistic load cases with respect to the other estimates; thus, SIA 261/1 loads were chosen as the reference for further analyses.

4.2. Linear Buckling Analysis (LBA)

An initial LBA on the tower was performed in order to localize potential failure points on the structure and provide buckling imperfections (scaled modal shapes) for the following non-linear analysis steps.

In this case, the LBA perturbations were the previously calculated wind load (self-weight of the structure was applied in a static pre-step and did not act as perturbation). As it is a quicker and more practical procedure, it was suited for finding which wind direction was the most unfavorable for the structure, even though it did only provide the onset of the instability and not the ultimate load capacity of the structure (which might depend on the post-buckling behavior, redundant structural elements, members that undergo yielding and inelastic buckling).

Different wind directions and magnitudes were analyzed by creating a series of load cases in Matlab [27] and implementing them in the FE model via an Abaqus Macro [20] function. The result of this analysis is displayed alongside the reference SIA 261/1 load case values in the polar plot in Figure 21 (depending on the wind angle of attack). Figure 22 shows the resulting modes from the LBA with transverse wind forcing (0°).

The unfavorable wind directions were between 12° and 26° in the transverse direction and the wind load in that direction could reach the ultimate load according to the LBA (between 1.00 to 1.04 times the LBA instability limit). The failure mode was always localized between the 7th and 8th, or on the 2nd level of the tower (Figure 22, reference Figure 19 for level numbering).

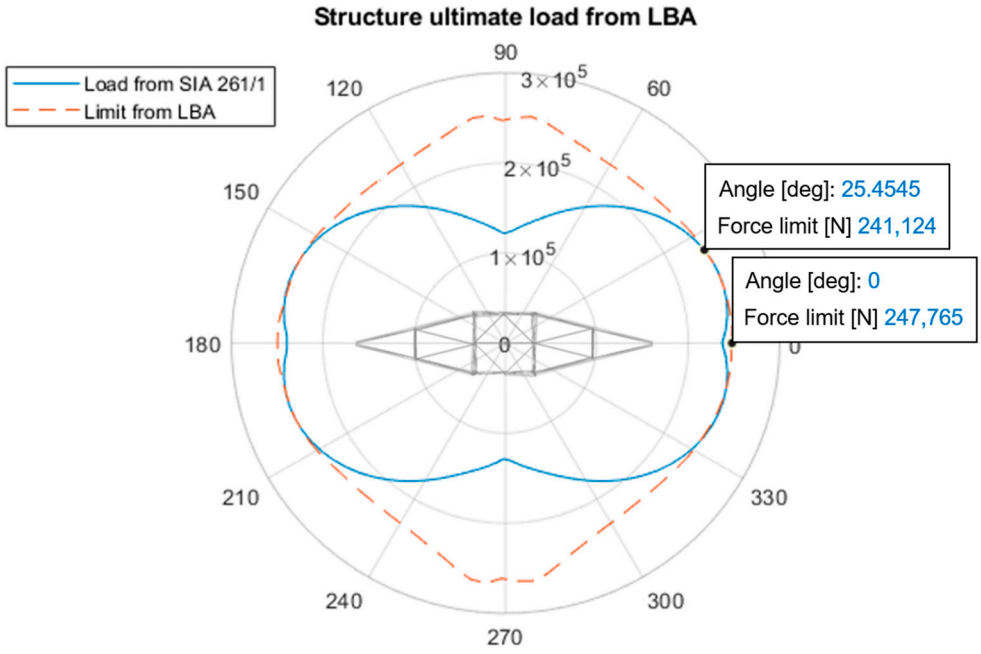
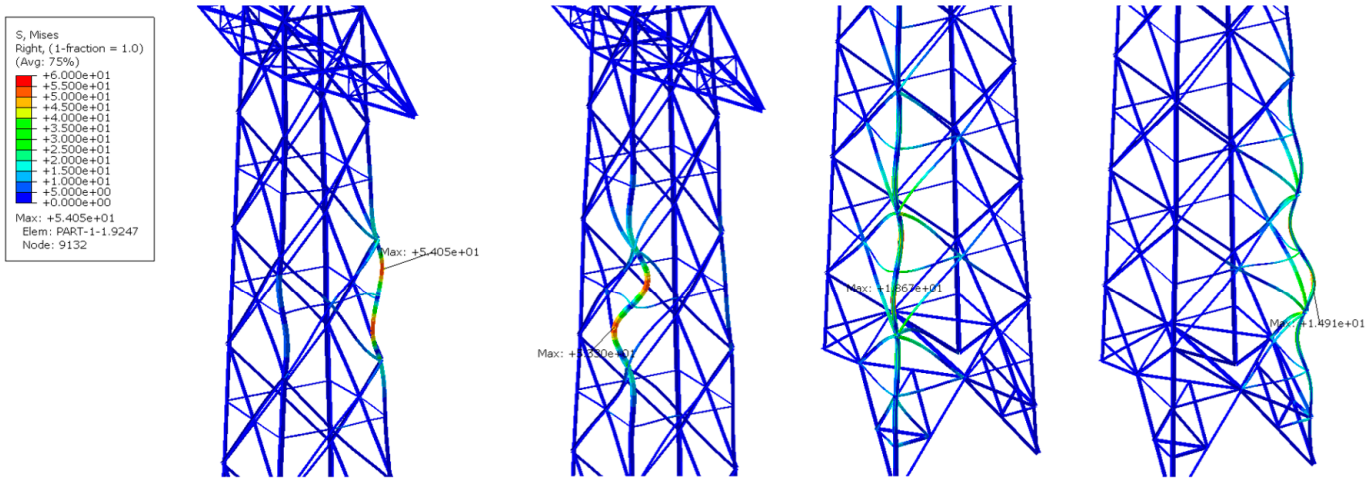


Figure 21. Instability load from LBA, in terms of total load (in N), compared with the SIA 261/1 load case. The LBA values at 0° and at 25.4° in the transverse direction, extremely close to the design load case, are highlighted.



Mode 1
Instability load:
236.56 kN

Mode 2
Instability load:
237.10 kN

Mode 3
Instability load:
502.68 kN

Mode 4
Instability load:
504.28 kN

Figure 22. Buckling modes shapes and instability loads from the LBA; results with transverse wind forcing (0°), scale factor = 500. The two pictures on the left show the failure at the 7th and 8th level of the tower, whereas the two on the right show the failure at the 2nd level.

4.3. Non-Linear Buckling Analysis with Imperfections

The RIKS procedure in Abaqus 2021 accounted for geometric imperfections and material non-linearities. A non-linear buckling analysis of this kind, based on the purely transverse wind load case (0°), was performed, proportionally increasing the load magnitude to estimate the maximum load-bearing capacity. The self-weight of the structure was also applied in a static pre-step and remained constant during the RIKS step.

As pointed out in Section 3, imperfections can significantly affect the load-bearing capacity of the structure. The studies of Piskoty et al. [28] and Wang et al. [14], who studied

the effects of superimposed buckling imperfections on the collapse—due to structural instabilities—of a roof and of a steel lattice tower, respectively, support this claim.

Eurocode 1993-3.1 [5] specifies a formula for standard imperfections to be applied during analysis: with $m = 668$ being the number of members of the bracing system, and $e_{imp} = L/706.5$.

Based on the literature, different imperfection modes were applied:

- superposition of buckling imperfections (scaled from mode 1, 2, 3 and 4 of the previous LBA, Figure 22) with magnitude $e_{imp} = L/706.5$, which is standard practice during design;
- the removal of secondary elements (before the initiation of the simulation), highlighted in Figure 23, while the impact of element removal on the tower capacity was also analyzed by Eslamlou et al. [29], but from the dynamic perspective;
- deformation of the supports with magnitude $e_{imp} = L/706.5$, the type of imperfections illustrated in Figure 24, which can be quite harmful to structural integrity, as proved Jian et al. [30] and Wang et al. [31], who both analyzed, via numerical methods, the effect of displacement on tower basement supports.

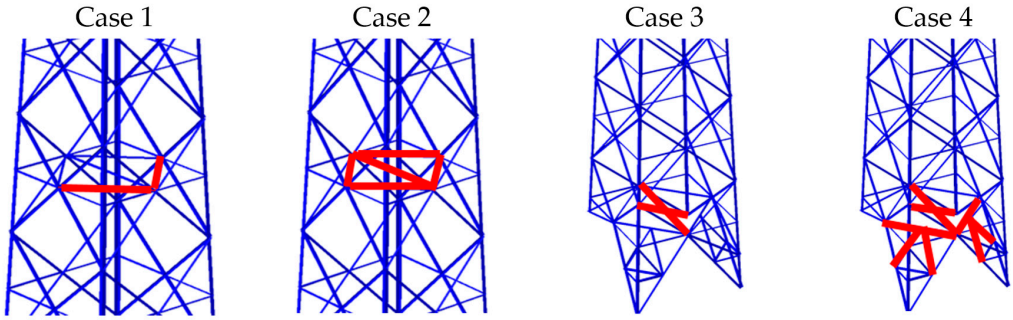


Figure 23. Highlighted: the removed secondary structural elements. Case 1 has 2 braces missing from the 5th level; Case 2 had 5 missings (the entire secondary structural reinforcement section); Case 3 had 2 braces missing from the 1st level; and Case 4 had 8 elements from the same level missing (in the legs).

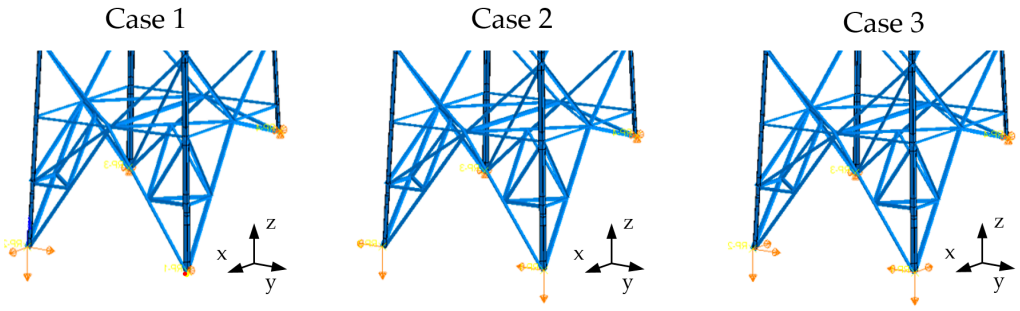


Figure 24. Support movement direction and magnitude for every analyzed case. In Case 1, a single leg was moved in x+ and y+ directions (positive displacements) and z- (negative disp.); in Case 2, two legs were moved in y- and z- directions (negative disp.); in Case 3, two legs were moved in x-, y- and z- directions (negative displacement). No support, including the ones that did not move, allowed rotation in any axis.

The results of the linear (LBA) and non-linear (RIKS) analysis can be found in Table 7, as a ratio, with respect to the reference SIA 261/1 load case.

The failure modes (Table 7, Figure 25) were similar to what was already evident in the LBA, but the ultimate load capacity was, in general, higher than modes 1 and 2 from the LBA (between 1 and 1.29 times the LBA mode 1 instability load, and between 1.04 and 1.35 times the reference load SIA 261/1 (Figure 26)): a section yielding, or redundant members,

might increase the capacity over the stability limit. Considering the failure at the 7th level alone, the ultimate load capacity ranged from 1.33 to 1.35 times the SIA 261/1 reference load case. At the 2nd level of the structure, the load capacity appeared to be more sensitive to imperfections, ranging from 1.04 to 1.23 times that of the reference, which is much lower than the instability value predicted by the LBA (>500 kN). The structures' sensitivity to imperfections was in the same range of variation of similar lattice structures failure cases [12–14,16–19,29–31]. The missing secondary structural elements did not appear to have a significant effect on the ultimate load capacity. The most unfavorable imperfection appeared to be the displacement of the basement legs, with case 1 resulting in the lowest load-bearing capacity. This load case was not based on standards or design guidelines, nor on measurements; therefore, it might have resulted in being too conservative. The lack of structural reinforcements did not appear to cause any variation in the load capacity of the tower. The superimposition of buckling imperfections had a similar impact. The failure was inelastic buckling-driven: only a small portion of the section was plasticized when the ultimate load was reached.

Table 7. Ultimate load capacity in LBA and RIKS analysis procedures, based on imperfections from Figures 22–24. Note that the reference design load case from SIA 261/1 is equivalent to a total load of 237.2 kN.

Analysis Procedure	Buckling Mode	Imperfection Mode	Ultimate Load Capacity (kN)	Failure (Level No.)
LBA	1, 2	-	247.7	7th
	3, 4	-	502.3	2nd
RIKS	-	Buckling mode 1, 2 (on 7th level)	313.9	7th
	-	Buckling mode 3, 4 (on 2nd level)	292.2	2nd
	-	Missing element, case 1	321.3	7th
	-	Missing element, case 2	320.9	7th
	-	Missing element, case 3	292.9	2nd
	-	Missing element, case 4	288.2	2nd
	-	Support displacement, case 1	246.8	2nd
	-	Support displacement, case 2	282.4	2nd
	-	Support displacement, case 3	314.9	7th

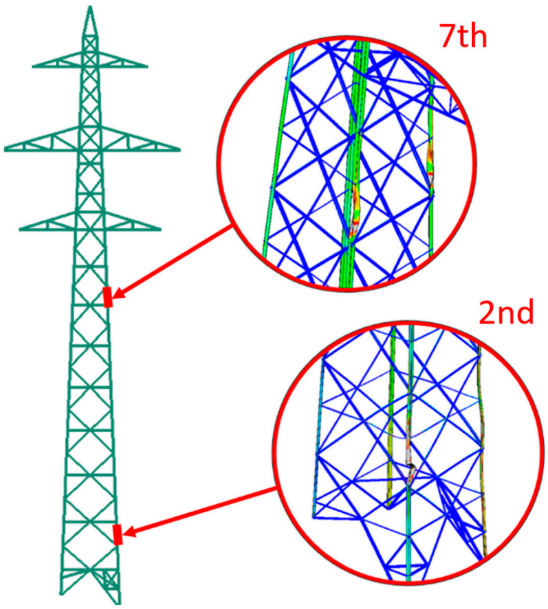


Figure 25. Failure positions at 7th and 2nd level are highlighted.

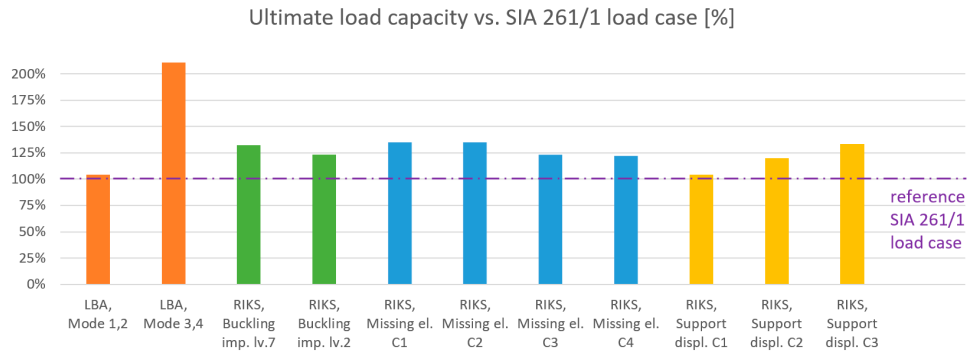


Figure 26. Ultimate load-bearing capacity in LBA and RIKS analysis versus the design load case from SIA 261/1 as a reference.

4.4. Non-Linear Post-Buckling Analysis

In order to obtain an estimation of the remaining capacity after the first failure, a post-buckling analysis (with RIKS procedure) was carried out in a model in which the failed elements of the 7th or the 2nd level (main legs, highlighted in Figure 25) were removed.

When removing the main legs elements from the 7th level, the tower's wind load capacity was reduced by 87.4%, whereas, when removing them from the 2nd level, the tower was not even able to withstand its own weight. The sudden collapse of the tower after the first elements failed is therefore plausible. Moreover, the damage remained localized (Figure 27); the additional damage found on the real towers could be attributed to the cascade sequence dynamic loads or to the contact with the ground.

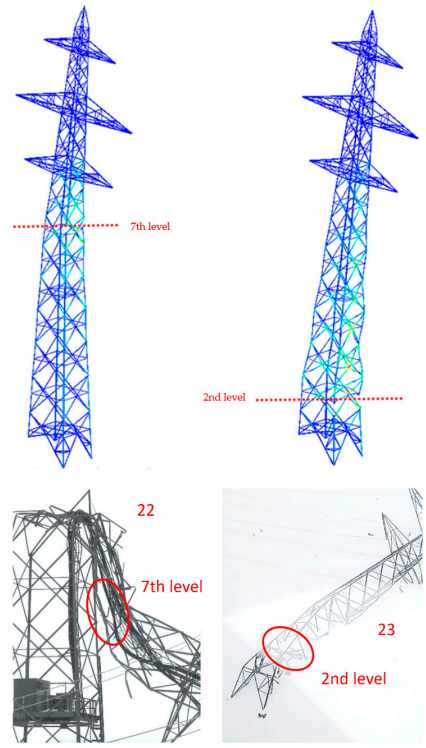


Figure 27. Post-buckling deformation compared against the real failure, at the 2nd level (on the right side) and 7th level (on the left side). Note that tower No. 23 (modeled) had the same upper structure (above the 5th section, reference Figure 19 for section numbering) as all the other towers in the line segment (including the No. 22 showed in the picture on the left); thus, it can be assumed that wind loads and failure modes in the upper part were the same in every tower.

5. Discussion

The use of joint compliance in the modeling of lattice structures can be a viable method to improve accuracy, but this requires a large number of parameters and modeling details which are partly based on several joint sub-models and their FE results in order to build the stiffness functions and determine the coefficients (as shown in Figure 8). Hence, modeling with fixed connections between lattice members was used for the analysis of the complete towers, which proved to be a more efficient and realistic representation in the proposed case, although this is based on the ideal assumption of infinite moment transfer through the joints. It might be a good tradeoff for computationally demanding models to partially build the lattice structure with compliant joints (for example, employing them in the most critical area only), or using pinned joints for single-bolt connections.

The load capacity calculated by the non-linear RIKS analysis was 1.0 to 1.29 times the values from LBA for the failure at the 7th level, which hints that section yielding or redundant members might increase the capacity over the instability limit. However, for the failure at the 2nd level, the non-linear RIKS predicts a load capacity as low as 51% of the corresponding LBA instability load (as this refers to the 3rd and 4th eigenmode), which indicates that non-linearities and applied imperfections can significantly affect the FE results. We can summarize from Table 7 that the "hidden reserve", i.e., the ratio of the collapse load to the stability limit (from the LBA), was in the range of 17 to 36% for rather standardized imperfections, and dropped to 4% for the case of a support displacement (case 1), meaning that our assumptions were too conservative and should be based on actual measurements.

The analysis further showed that the towers were quite close to their ultimate capacity, even under a rather moderate load case of static wind pressure (not considering any turbulences). The narrow safety margin (4% to 36%) with respect to SIA 261/1 (Figure 26) means that the calculated load capacity of the structure would only be in the range of 62 to 82% for more conservative design loads, e.g., according to EN 1991-1-4. Moreover, the following aspects should be considered:

- EN 1991-1-4 wind pressure values account for dynamic peak load (in Figures 19 and 20, the "Mean" value from Figure 17 is used instead), whereas SIA 261/1 does not.
- The higher base wind pressure value of 3.3 kPa in the weather map (Figure 16) is recommended during design, instead of the lower value of 1.1 kPa used for this analysis, which would increase the total loads in Figures 19 and 20 by three times (no matter what design standard load case is considered).

In addition, the wide range of wind pressure present in the Swiss standards (Figure 16) provokes a significant uncertainty in the load assumptions. Updated localized weather data could drastically improve the design of power transmission lines, without the risk of overdesigning exposed structures.

Overall, the structures' sensitivity to imperfections was in the same range as has been proved in similar failure cases of lattice structures [12–14,16–19,29–31], but the model accuracy could not be further assessed: validation procedures were not available, as testing on large lattice structures is expensive and not economically viable in the context of such a project.

6. Conclusions

This study proposes modeling methods for lattice towers affected by structural instability under wind loading, with the final purpose of being applied to a failure analysis case, specifically in the estimation of ultimate load capacity and failure position.

In general, the following conclusions can be drawn with regard to modeling approaches to structural instabilities:

- The proper use of element type and a minimum element size can increase the type of buckling modes that the model is able to display. However, there is no generalized "optimal" approach to the problem: a tradeoff between model accuracy and complexity

(proportional to computational cost) has to be achieved. Where allowed by the model complexity (i.e., for single braces with compliant joints, or for low-size assemblies), the best result is achieved with 3D elements, which are able to better simulate the complete joint friction interaction and the yielding of the section. When analyzing more computationally demanding models, structural elements (beam or shell) should be used, and the modeling of the joint compliance can improve the accuracy.

- Imperfections (in terms of magnitude and direction) can affect the instability mode and load of a structure. They should be measured during buckling experimental testing in order to provide more detailed input in the FE model, as well as in the design process.
- The geometric imperfections to be considered for complex structures are generally more standardized (mainly the eccentricities of trusses and beams), whereas load imperfections or the motion of the support (foundation) have to be measured or governed by product standards.
- The correct simulation of boundary conditions (i.e., joint compliance) largely improves both the single beam and lattice structure's instability mode and load estimation, and should be better accounted for in the standards. The pinned joint connection often employed in the design phase might not be a correct representation and can lead both to the underestimation of single-member capacity and to incorrect failure mode prediction (Sections 3.3 and 3.4).

The analysis proved that the wind alone can cause such a failure on the lattice structures in Albula Pass and the critical structural elements were correctly identified. Especially if the towers were designed based on the SIA 261/1 standard, with its base wind pressure of 1.1 kPa, at the time of their erection, they were rather under-designed for the exceptional windstorm event which occurred ("one in a century"). The present study only considered constantly blowing wind, as there was no information or measured data on wind gusts and turbulences. Even with these 'optimistic' assumptions, the collapse could be proved just with the lower range of plausible wind scenarios, i.e., constant wind acc. to the lowest pressure levels in the standard. Hence, the presence (and consideration) of additional turbulences would have only speeded up the collapse.

The high sensitivity to the applied imperfections caused the ultimate load capacity to range between 117% and 136% of the reference load case (104% for the hypothetical and exceptional case of a displacement of the foundation). According to the static non-linear analysis, the elements most likely to have failed first were located at the 2nd level and the 7th level of the structure (the main 'legs' of the towers), as they were closer to their limit when realistic imperfections are applied, and they were found broken in the real structures. The non-linear post-buckling analysis proved that the tower could have suddenly collapsed after the main leg sections failed, as this means it would have lost almost all the load-bearing capacity.

The towers were quite close to their ultimate capacity even under a rather moderate static load case (a safety margin of just 4% to 36% with respect to SIA 261/1, Table 7 and Figure 26). It is nevertheless not advisable to generally increase the safety factors for the design of such lattice structures, but rather, to make refined load assumptions which take better account of local conditions (e.g., by the long-term measurement of the local weather conditions). Probabilistic analyses and fragility analyses, as suggested by Hughes et al. [32], may be applied to obtain more local and customized load assumptions, which allow us to consider combinations of statistical deviations in the input parameters of the design models.

Author Contributions: G.V. developed the analysis models and produced most of the results. He implemented a Matlab code to apply the load cases to the FE model based on the assumptions for wind direction and pressure. Z.L. provided valuable input in joint modelling, non-linear analysis procedures and the validation of the numerical results. He was also involved in further software development (Matlab and Abaqus user subroutines). Finally, he was a great support in writing and reviewing of the manuscript. C.A. led the failure analysis, was responsible for the conceptualization and the applied methodology for the present work, and took care of supervision and project administration. All authors have read and agreed to the published version of the manuscript.

Funding: This research received no external funding.

Data Availability Statement: No available dataset was created.

Acknowledgments: We thank Sandro Dinser for his support during the project and many fruitful discussions.

Conflicts of Interest: The authors declare no conflict of interest.

References

1. Campbell, R.J.; Lowry, S. *Weather-Related Power Outages and Electric System Resiliency, 2012: Congressional Research Service*; Library of Congress: Washington, DC, USA, 2012.
2. Hoffman, P.; Bryan, W. *Comparing the Impacts of Northeast Hurricanes on Energy Infrastructure*; Us Department of Energy: Washington, DC, USA, 2013.
3. Fang, S.J.; Roy, S.; Kramer, J. Transmission structures. In *Structural Engineering Handbook*; Mcgraw-Hill Companies: New York, NY, USA, 1999. Available online: https://www.yumpu.com/en/document/read/47078899/fang-sj-roy-s-and-kramer-j-transmission-structures-free/ (accessed on 16 April 2022).
4. *EN 1993-1-1*; Eurocode 3: Design of Steel Structures—Part 1-1. General Rules and Rules for Buildings. European Standard. 2005. Available online: https://www.phd.eng.br/wp-content/uploads/2015/12/en.1993.1.1.2005.pdf (accessed on 2 January 2023).
5. *EN 1993-3-1*; Eurocode 3: Design of Steel Structures—Part 3-1. Towers, Masts and Chimneys—Towers and Masts. European Standard. 2006. Available online: http://www.iso-iran.ir/standards/bs/BS_EN_1993_3_1_2009_,_Eurocode_3.pdf (accessed on 2 January 2023).
6. *EN 50341-1*; Overhead Electrical Lines Exceeding Ac 1 Kv Part 1. General Requirements Common Specifications. Ics 29.240.20. European Standard. 2013. Available online: https://www.en-standard.eu/une-en-50341-1-2017-overhead-electrical-lines-exceeding-ac-1-kv-part-1-general-requirements-common-specifications/ (accessed on 1 May 2022).
7. *RS 734.31*; Electrical Wiring Regulation (Verordnung über Elektrische Leitungen) (German), Schweizerischen Bundesrat. The Swiss Federal Council: Switzerland, 1994. Available online: https://www.fedlex.admin.ch/eli/cc/1994/1233_1233_1233/de/ (accessed on 1 May 2022).
8. *SIA 261/1*; Actions on Structures—Supplementary Specifications (German), Herausgeber Schweizerischer Ingenieur- Und Architektenverein Postfach, Ch-8039 Zürich. Swiss Society of Engineers and Architects. 2003. Available online: https://iisee.kenken.go.jp/worldlist/50_Switzerland/50_Switzerland_Code.pdf (accessed on 2 January 2023).
9. *PLS-CADD User Manual, Version 16.0*; Power Line Systems: Madison, WI, USA, 2019.
10. Kettler, M.; Lichtl, G.; Unterweger, H. Experimental Tests on Bolted Steel Angles in Compression with Varying End Supports. *J. Constr. Steel Res.* **2019**, *155*, 301–315. [CrossRef]
11. Kettler, M.; Unterweger, H.; Zauchner, P. Design Model for Bolted Angle Members in Compression Including Joint Stiffness. *J. Constr. Steel Res.* **2021**, *184*, 106778. (In English) [CrossRef]
12. Albermani, F.; Kitipornchai, S.; Chan, R.W.K. Failure Analysis of Transmission Towers. *Eng. Fail. Anal.* **2009**, *16*, 1922–1928. [CrossRef]
13. Alminhana, F.; Mason, M.; Albermani, F. A Compact Nonlinear Dynamic Analysis Technique for Transmission Line Cascades. *Eng. Struct.* **2018**, *158*, 164–174. [CrossRef]
14. Wang, J.; Li, H.-N.; Fu, X.; Li, Q. Geometric Imperfections and Ultimate Capacity Analysis of a Steel Lattice Transmission Tower. *J. Constr. Steel Res.* **2021**, *183*, 106734. [CrossRef]
15. Affolter, C.; Piskoty, G.; Wullschleger, L.; Weisse, B. Collapse of A High Storage Rack. *Eng. Fail. Anal.* **2009**, *16*, 1846–1855. [CrossRef]
16. Rao Prasad, N.; Knight, G.M.S.; Lakshmanan, N.; Iyer, N.R. Investigation of Transmission Line Tower Failures. *Eng. Fail. Anal.* **2010**, *17*, 1127–1141. [CrossRef]
17. Prasad, N.R.; Samuel Knight, G.M.; Seetharaman, S.; Lakshmanan, N.; Iyer, N.R. Failure Analysis of Transmission Line Towers. *J. Perform. Constr. Facil.* **2011**, *25*, 231–240. [CrossRef]
18. Prasad, N.R.; Knight Samuel, G.M.; Mohan, S.J.; Lakshmanan, N. Studies on Failure of Transmission Line Towers In Testing. *Eng. Struct.* **2012**, *35*, 55–70. [CrossRef]
19. Mohammadi, Y.D.; Shafieezadeh, A.; Cha, K. Effect of Modelling Complexities on Extreme Wind Hazard Performance Of Steel Lattice Transmission Towers. *Struct. Infrastruct. Eng.* **2019**, *16*, 898–915. [CrossRef]
20. Abaqus 2021 Analysis User's Manual; Simulia: Providence, RI, USA, 2021. Available online: https://www.3ds.com/support/hardware-and-software/simulia-system-information/abaqus-2021/ (accessed on 15 May 2022).
21. Uriz, P.; Filippou, F.C.; Mahin, S.A. Model for Cyclic Inelastic Buckling of Steel Braces. *J. Struct. Eng.* **2008**, *134*, 619–628. [CrossRef]
22. Beer, F.P., Jr.; Dewolf, J.T. *Mechanics of Materials*, 6th ed.; Mcgraw-Hill Companies: New York, NY, USA, 2012.
23. *EN 1993-1-8*; Eurocode 3: Design of Steel Structures—Part 1-8: Design of Joints. European Standard. 2005. Available online: https://www.phd.eng.br/wp-content/uploads/2015/12/en.1993.1.8.2005-1.pdf (accessed on 2 January 2023).

24. *EN 1991-1-4*; Eurocode 1: Actions on Structures—Part 1-4: General Actions—Wind Actions. European Standard. 2005. Available online: https://www.phd.eng.br/wp-content/uploads/2015/12/en.1991.1.4.2005.pdf (accessed on 2 January 2023).
25. Prud'homme, S.; Legeron, F.; Langlois, S. Calculation of Wind Forces on Lattice Structures Made of Round Bars by A Local Approach. *Eng. Struct.* **2018**, *156*, 548–555. [CrossRef]
26. Stroman, J.C. *Aerodynamic Drag Coefficients of a Variety of Electrical Conductors*; Graduate Faculty of Texas Tech University: Lubbock, TX, USA, 1997.
27. *Matlab, Version 9.9*; The Mathworks Inc.: Natick, MA, USA, 2020.
28. Piskoty, G.; Wullschleger, L.; Loser, R.; Herwig, A.; Tuchschmid, M.; Terrasi, G. Failure Analysis of a Collapsed Flat Gymnasium Roof. *Eng. Fail. Anal.* **2013**, *35*, 104–113. [CrossRef]
29. Eslamlou, S.D.; Asgarian, B. Determining Critical Areas of Transmission Towers Due to Sudden Removal of Members. *Case Stud. Eng. Fail. Anal.* **2017**, *9*, 138–147. [CrossRef]
30. Jian, M.; Zhang, G.; Zhang, D.; Liu, G.; Fan, Z. Analysis of Uneven Settlement and Restoration Measures for One 220kv Transmission Tower. In *2015 2nd International Forum on Electrical Engineering and Automation (Ifeea 2015)*; Atlantis Press: Paris, France, 2016; pp. 249–252.
31. Wang, W.; Li, H.; Tian, L. Progressive Collapse Analysis of Transmission Tower-Line System Under Earthquake. *Adv. Steel Constr.* **2013**, *9*, 161–172.
32. Hughes, W.; Zhang, W.; Lu, Q. Fragility Analysis of Transmission Tower-Line System under Multiple Environmental Loadings. In Proceedings of the Electrical Transmission and Substation Structures Conference, Orlando, FL, USA, 2–6 October 2022; pp. 207–222.

Disclaimer/Publisher's Note: The statements, opinions and data contained in all publications are solely those of the individual author(s) and contributor(s) and not of MDPI and/or the editor(s). MDPI and/or the editor(s) disclaim responsibility for any injury to people or property resulting from any ideas, methods, instructions or products referred to in the content.